PHYSICAL REVIEW D VOLUME 36, NUMBER 9 1 NOVEMBER 1987

Statistical properties of cosmic-ray showers at ground level determined from photomultiplier-tube background registrations

Malvin C. Teich
Center for Telecommunications Research and Department of Electrical Engineering, Columbia University, New York, New York 10027

Richard A. Campos
Columbia Radiation Laboratory and Department of Applied Physics, Columbia University, New York, New York 10027

Bahaa E. A. Saleh
Department of Electrical and Computer Engineering, University of Wisconsin, Madison, Wisconsin 53706
(Received 10 March 1987)

The fluctuations of cosmic-ray particles resulting from extensive air showers at ground level are well described by the two-parameter Poisson-driven Yule-Furry and negative-binomial counting probability distributions. The background signal from a single photomultiplier tube has been used to experimentally verify these results with remarkable precision, in spite of the simplicity of the underlying pure-birth stochastic process. Counting distributions from three different photomultiplier-tube detectors operated in the dark are presented, together with the theoretical predictions. Probability distributions of interevent times have also been obtained and these are found to be consistent with the observed clustering properties at the detector output. Our approach is expected to be of importance in quantum optics where cosmic-ray-shower particles can pose a significant limitation on the detection of squeezed light.

I. INTRODUCTION

The rich historical legacy embodied by cosmic-ray research began in 1912 when the extraterrestrial origin of ionizing radiation in the atmosphere was inferred from the pioneering balloon experiments of Victor Hess. By recording their tracks in triggered cloud chambers, Rossi[1] and others demonstrated that some cosmic rays at ground level can initiate cascades and are stopped in thin lead plates, while others continue to penetrate through much thicker layers of the same material without multiplicative effects (hence the designations soft and hard components, respectively). The penetrating power of the latter revealed for the first time the existence of carriers of ultrahigh energies and heralded the search for new elementary particles, thus opening an important chapter in modern physics.

The fate of primary cosmic-ray particles from space determines the duality of observed behavior in lead, as is now well understood. The primary particles (consisting mostly of protons) collide soon after entering Earth's atmosphere and fragment into metastable species such as π mesons, which propagate the Yukawa strong force beyond the interaction region. If not captured, the charged pions decay readily into inert μ mesons that collide infrequently and survive to the ground as the penetrating facet of the cosmic radiation.[2] Muons may also disintegrate over a relatively long time span into electrons or positrons, in accordance with their initial charge state. The neutral pions, on the other hand, are much more unstable than their charged counterparts and decay swiftly into photon pairs.

These resulting photons and the less abundant muon-derived electrons are seeds of the atmospheric avalanche effect, and, thus, collectively encompass the multiplicative nature of cosmic rays. A single high-energy photon in matter may materialize into an electron-positron pair, whose members in turn radiate further photons through bremsstrahlung collisions. A cyclic mechanism is thus available to initiate and sustain an electromagnetic cascade where the energy of the source particle is partitioned among its offspring until the individual share is low enough for Compton scattering, ionization losses, and other processes to dominate and dilute the avalanche. If the source is sufficiently energetic, however, the family survives down to ground level where it can be detected as an extensive air shower.[3]

It is the statistical behavior of this cascading component of the cosmic-ray progeny that is of principal interest in this paper. We focus on the fluctuations in shower size that arise from the inherent randomness of the multiplication processes, rather than on the distribution of secondary-particle energies. The mathematical description is rooted in stochastic branching-process theory.

From the unfolding history of a primary cosmic ray in the atmosphere, we can clearly identify at least three levels of randomness. They represent the fluctuations in primary arrivals, in the number of cascade-initiating sources per primary, and in the population of each such cascade. For greatest simplicity, however, we eliminate the intermediate level of random behavior and assume

that a primary cosmic ray collisionally excites only a single shower.

We employ the Poisson-driven Yule-Furry and negative-binomial counting probability distributions, which are derived in the context of cascade theory in the next section, to describe the fluctuations of cosmic-ray showers at ground level. To demonstrate the efficacy of these models, we present in Sec. III experimental counting distributions, which were generated in the dark from ordinary photomultiplier tubes, over a broad range of counting times and experimental durations.

II. THEORY OF COSMIC-RAY-SHOWER STATISTICS

A. Showers initiated by a single primary event

The first statistical treatment of a single-primary-event cascade as applied to cosmic rays was presented by Bhabha and Heitler[4] in the United Kingdom and simultaneously by Carlson and Oppenheimer[5] in the United States. The model is equivalent to a zero-memory process whereby daughter particles are independently added to the cascade. In a counting experiment, this model leads to a Poisson-distributed number of secondaries,[6,7] i.e.,

$$P(k;T)=\langle k\rangle^{k}\exp(-\langle k\rangle)/k!, \quad k\geq 0 . \tag{1}$$

The angular brackets denote an ensemble average and T is the counting time, which is chosen to be sufficiently long to capture the entire cluster of secondary events, so their nonstationary production can be effectively treated as instantaneous. In other words, if t_s is the temporal spread of the cluster, then the requirement $T\gg t_s$ ensures that no events are lost to the counting process. We assume this to hold henceforth.

Clearly the conservation laws that link the participants in the pair-production and bremsstrahlung processes would appear to suggest that the addition of new individuals to the cascade in an uncorrelated manner is inadequate. We have included the Poisson law in our discussion because of its broad applicability and its unique and fundamental property

$$\langle k\rangle=V(k)=M_3(k) . \tag{2}$$

Here V and M_3 denote the variance and third central moment of the distribution, respectively. We employ the Fano factor, defined as the variance-to-mean ratio, as an elementary measure of event dispersion.[8] The Fano factor $F_k(T)$ of the above Poisson counting distribution provides a convenient standard for comparison with other distributions, as it is simply given by

$$F_k(T)\equiv V(k)/\langle k\rangle=1 . \tag{3}$$

The inclusion of the primary particle in the shower statistics can be easily effected by a unit translation of the counting distribution of the secondaries

$$P(m;T)=P(k=m-1;T) , \tag{4}$$

yielding, in the above case, a shifted-Poisson (one-parameter) distribution for the shower size or multiplication m. Thus,

$$P(m;T)=\langle k\rangle^{m-1}\exp(-\langle k\rangle)/(m-1)! , \quad m\geq 1 , \tag{5}$$

where the mean value of the shifted distribution, $\langle m\rangle=\langle k\rangle+1$, reflects the deterministic addition of the primary particle to the fluctuating number of secondary events. Since the count variance is unchanged, the Fano factor becomes

$$F_m(T)=(\langle m\rangle-1)/\langle m\rangle=1-\exp(-\alpha) , \quad \alpha\geq 0 , \tag{6}$$

where we have set $\langle m\rangle=\exp(\alpha)$. The reason for this choice of notation will soon be apparent. Note that the Fano factor now approaches unity asymptotically with increasing α as the primary's determinism becomes largely obscured by the growing fluctuations of secondary counts.

The assumptions of this simple model were challenged by Furry[9] soon after their publication. In his landmark paper, Furry considered a pure-birth model whereby each cascade particle may directly breed daughters via a fixed birth rate λ. The multiplication then follows a shifted-geometric (shifted-Bose-Einstein) one-parameter counting distribution

$$P(m;T)=\exp(-\beta)[1-\exp(-\beta)]^{m-1} , \quad \beta\geq 0,\ m\geq 1 . \tag{7}$$

The statistics up to third order are

$$\langle m\rangle=\exp(\beta) , \tag{8a}$$

$$V(m)=\langle m\rangle^2-\langle m\rangle , \tag{8b}$$

$$M_3(m)=\langle m\rangle-3\langle m\rangle^2+2\langle m\rangle^3 ; \tag{8c}$$

the Fano factor is, therefore,

$$F_m(T)=\exp(\beta)-1 . \tag{9}$$

Here the unitless branching parameter $\beta=\lambda t_s$ is the product of the growth rate λ and the clusters playout time t_s. Hence when $t_s=0$ there is no branching, since only the primary event is present, but the mean multiplication subsequently grows exponentially with t_s. The quantity α in Eq. (6) can now be viewed as an equivalent branching-process parametrization of the shifted Poisson distribution.

The above counting distribution was independently derived earlier by Yule in connection with his elegant mathematical treatment of evolution.[10] An exact parallel follows if we identify the shower population as the number of species within a genus and if we let the branching mechanism represent random mutations. The shifted-Bose-Einstein counting distribution is, therefore, also known as the Yule-Furry distribution, and the point process from which it is derived is termed a Yule-Furry process.

Finally, we examine the use of a related model whose mathematical properties resemble those of the Yule-Furry distribution. This is the one-parameter logarithmic counting distribution

$$P(m;T)=(1/\theta)(q^m/m), \quad 0\le q\le 1,\ m\ge 1\ , \tag{10a}$$

$$\theta=\ln[1/(1-q)]\ , \tag{10b}$$

where θ is a normalization factor. We can rewrite this distribution, in terms of θ, into the suggestive form

$$P(m;T)=[1-\exp(-\theta)]^m/\theta m, \quad \theta\ge 0,\ m\ge 1\ , \tag{11}$$

with statistics, up to third order,

$$\langle m\rangle=(1/\theta)[\exp(\theta)-1]\ , \tag{12a}$$

$$V(m)=\langle m\rangle+(\theta-1)\langle m\rangle^2\ , \tag{12b}$$

$$M_3(m)=\langle m\rangle+3(\theta-1)\langle m\rangle^2+(2\theta^2-3\theta+2)\langle m\rangle^3\ . \tag{12c}$$

The corresponding Fano factor is

$$F_m(T)=1+[(\theta-1)/\theta][\exp(\theta)-1]\ . \tag{13}$$

The striking similarity between the Yule-Furry and logarithmic statistics is not accidental. As shown in Appendix A, these counting distributions are in fact related when $\theta=\beta$, although statistical equality does not follow from this condition [as is evident from Eqs. (8a) and (12a)]. Nevertheless, we may mimic the evolution of the Yule-Furry mean multiplication by setting

$$\langle m\rangle=(1/\theta)[\exp(\theta)-1]=\exp(\gamma)\ , \tag{14}$$

which is a transcendental equation for $\theta=f(\gamma)$. The dependence of the Fano factor on γ cannot be determined analytically, although this poses no difficulty since for a given value of γ we may obtain the corresponding value of θ (and, hence, the Fano factor) from a numerical table.

The advantage of this technique rests on the mathematical equivalence of the parameter γ to α and β, which allows us to present the associated Fano-factor dependencies together for comparison in Fig. 1(a). In contrast with the asymptotic Fano factor of the shifted-Poisson counting distribution, the Fano factors for the Yule-Furry and logarithmic counting distributions follow a similar trend and rise quickly with increasing multiplication. The latter two models thus allow us to describe the clustered behavior of cosmic-ray showers for large multiplication with far greater accuracy than the former. The principal underlying reason is the association of parents to their offspring at each branching stage of the multiplicative process.

Representative probability distributions are presented in Fig. 1(b) for $\langle m\rangle=1.005$, 1.2, and 3.0. Note that in this, and all counting distributions to follow, the theoretical values are shown as continuous curves for clarity, but they have significance only at the discrete values of the count index. It is clear that for fixed multiplication the logarithmic distribution exhibits greater variance than the Yule-Furry distribution; however, all three models converge to an equivalent description for very low multiplication. This is also apparent in Fig. 1(a).

We conclude this section by speculating on the validity of the Yule-Furry distribution in describing the soft component of the cosmic-ray progeny. Clearly the model represents only a first-order idealization of the problem since it considers only a single particle species (hence, not accounting for the alternating generations of electrons and photons in the physical cascade), and, as a pure-birth process, it does not incorporate particle losses and immigration.

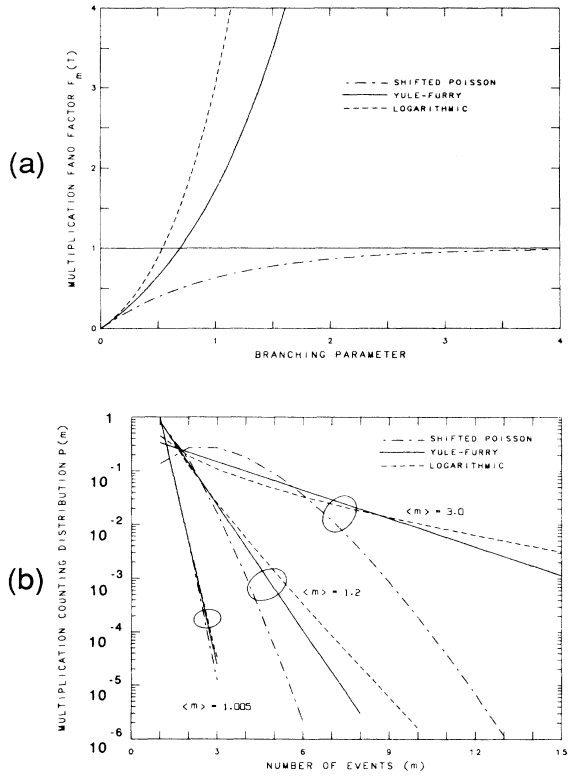

FIG. 1. (a) Multiplication Fano factor $F_m(T)\equiv V(m)/\langle m\rangle$ versus branching parameter for three models of a cascade that is initiated by a single primary particle. The Fano factors of the Yule-Furry (solid curve) and logarithmic (dashed curve) counting distributions increase rapidly with branching parameter, in contrast with the bounded Fano factor of the shifted-Poisson (dashed-dotted curve) counting distribution. The former two models thus provide a more accurate description of cosmic-ray shower fluctuations. (b) Representative multiplication counting distributions $P(m;T)$ versus number of multiplication events m for the models of (a) with $\langle m\rangle=1.005$, 1.2, and 3.0. Although all three models are equivalent at low mean multiplication, the Yule-Furry and logarithmic differ substantially from the shifted-Poisson counting distribution as $\langle m\rangle$ increases. The tails of distributions for the former two models become much more developed than the latter, thus incorporating cascades with a larger number of events.

Extensions of the Yule-Furry have been considered by Arley[11] and Srinivasan[12] in their authoritative monographs. The framework for more sophisticated cascade treatments can be constructed from the general problem of birth, death, and immigration with time-dependent rates.[13] When no immigration is allowed, the mean and variance of the multiplication can be written more succinctly, yet with no loss of generality, as

$$\langle m \rangle = I(t_s) , \tag{15a}$$

$$V(m) = \langle m \rangle + \langle m \rangle^2 \left[2 \int_0^{t_s} \frac{\lambda(t)dt}{I(t)} - 1 \right] , \tag{15b}$$

where

$$I(t) = \exp \left[\int_0^t [\lambda(t') - \nu(t')] dt' \right] , \tag{15c}$$

where $\lambda(t)$ and $\nu(t)$ are the birth and death rates, respectively. Setting $\nu(t)=0$ and $\lambda(t)=\lambda$ reproduces the Yule-Furry results presented in Eqs. (8a) and (8b).

The temporal variation of these rates can be appropriately chosen to represent the degradation in offspring production due to the partitioning of energy among the particles of a developing cascade. Arley considered a simple example in which the death rate is linearly infused [$\nu(t)=\nu t$] while the birth rate is held constant [$\lambda(t)=\lambda$]. The evolution of the mean multiplication can be solved using Eq. (15a):

$$\langle m \rangle = \exp(\lambda t_s) \exp(-\nu t_s^2/2) . \tag{16}$$

This is the same result as that for a birth process that attenuates via the tail of a zero-mean Gaussian envelope with the standard deviation $\sigma = \sqrt{1/\nu}$. Since more energetic primaries yield larger showers, the Gaussian modulation can further be made dependent on the total primary energy by proper adjustment of the death-rate slope ν.

Apparently, the simple geometric character of the Yule-Furry pure-birth solution offers the essential ingredient for the characterization of cosmic-ray showers, regardless of the level of sophistication incorporated into the cascade model. Arley appreciated this and suggested that "... the region of validity of the simplifying approximations, of which any theory must necessarily make use, is always far wider than might be justified by theoretical arguments."

Mathematically, cascade counting distributions support a multiplication variance term that is proportional to the square of the mean. This is evident in Eq. (15b) for arbitrary birth and death rates. In the hierarchy of discrete probability distributions, the Bose-Einstein distribution (as well as its shifted version, the Yule-Furry) provides the simplest example of mean-square excess fluctuations. Our intuition regarding the logarithmic description of the multiplication is based on the presence of a similar dependence, as can be inferred from Eq. (12b).

B. Showers initiated by a Poisson number of primaries

We now generalize the results of the previous section by considering a number of primary events p, which is randomized via a suitable counting distribution $P(p;T)$. Since each primary event independently multiplies according to a model counting distribution $P(m;T)$, the overall cascade is an example of a compound process with well-known properties. In particular, the moment-generating function $Q_c(s)$ of the overall cascade counting distribution can be obtained by nesting those of the primary and multiplication counting distributions according to

$$Q_c(s) = Q_p(-\ln Q_m(s)) , \tag{17}$$

where the moment-generating function (MGF) is defined as

$$Q_x(s) \equiv \langle \exp(-sx) \rangle = \sum_{x=0}^{\infty} \exp(-sx) P(x;T) , \tag{18}$$

for a general counting process x (Ref. 14).

We can use the above result to obtain a useful set of equations that expresses the mean, variance, and third central moment of the overall cascade counting distributions $P(n_c;T)$ in terms of those of the constituent counting processes:

$$\langle n_c \rangle = \langle p \rangle \langle m \rangle , \tag{19a}$$

$$V(n_c) = V(p) \langle m \rangle^2 + \langle p \rangle V(m) , \tag{19b}$$

$$M_3(n_c) = M_3(p) \langle m \rangle^3 + 3V(p) \langle m \rangle V(m) + \langle p \rangle M_3(m) . \tag{19c}$$

These results are quite general and are explicitly derived in Appendix B. The former two expressions were first proved by Shockley and Pierce,[15] and the second is known as the cascade variance theorem.[16] Equation (19c) is an extension to third-order statistics; higher-order theorems are discussed via an equivalent method by Shih[17] in his treatment of hadronic multiplicity distributions.

If we now specify that the primaries arrive in *stationary* (or homogeneous) Poisson form, Eq. (19) simplifies considerably. We denote the mean of the primary Poisson distribution $\langle p \rangle$ as $\mu_p T$, where generally μ is the rate parameter of the homogeneous Poisson point process (HPP) and T is the counting time over which we observe the events. For the Poisson primaries, we then have $\langle p \rangle = V(p) = M_3(p) = \mu_p T$, whereupon

$$\langle n_c \rangle = \mu_p T \langle m \rangle , \tag{20a}$$

$$V(n_c) = \mu_p T [\langle m \rangle^2 + V(m)] , \tag{20b}$$

$$M_3(n_c) = \mu_p T [\langle m \rangle^3 + 3 \langle m \rangle V(m) + M_3(m)] . \tag{20c}$$

This can be compactly rearranged in terms of the ordinary moments as

$$\langle n_c \rangle = \mu_p T \langle m \rangle , \tag{21a}$$

$$V(n_c) = \mu_p T \langle m^2 \rangle , \tag{21b}$$

$$M_3(n_c) = \mu_p T \langle m^3 \rangle . \tag{21c}$$

The Fano factor is given by

$$F_c(T) = \langle m \rangle + F_m(T) , \tag{22}$$

and depends solely on the multiplication statistics.

For the case of a primary Poisson counting distribution with Yule-Furry multiplication, we use Eq. (8) in Eq. (20) to provide the overall cascade statistics, up to third order:

$$\langle n_c \rangle = \mu_p T \exp(\beta) , \tag{23a}$$

$$V(n_c) = \mu_p T \exp(\beta) [2 \exp(\beta) - 1] , \tag{23b}$$

$$M_3(n_c)=\mu_p T\exp(\beta)[6\exp(2\beta)-6\exp(\beta)+1]\ . \tag{23c}$$

These formulas are appropriate for the Poisson-driven Yule-Furry (PDYF) counting distribution, which has been shown to obey the recursion relation[18,19]

$$P(n_c+1;T)=\frac{\langle n_c\rangle}{n_c+1}\sum_{k=0}^{n_c}P(n_c-k;T)A(k)\ , \tag{24a}$$

$$A(k)=(k+1)\exp(-2\beta)[1-\exp(-\beta)]^k\ , \tag{24b}$$

with the initial condition

$$P(0;T)=\exp(-\mu_p T)\ . \tag{24c}$$

Equation (24c) indicates that the probability of observing zero cascade counts is simply the probability of arrival of zero primaries in the counting interval. Note also that as $\beta\rightarrow 0$ this recursion relation reduces to that for the Poisson law of the primaries.

Finally, we consider the case of logarithmic multiplication with statistics given by Eq. (12). Utilizing Eq. (20) once more and using the transformation

$$\langle n_0\rangle=\mu_p T[\exp(\theta)-1]/\theta\ , \tag{25a}$$

$$M=\mu_p T/\theta\ , \tag{25b}$$

we find

$$\langle n_c\rangle=\langle n_0\rangle\ , \tag{26a}$$

$$V(n_c)=\langle n_0\rangle[1+(\langle n_0\rangle/M)]\ , \tag{26b}$$

$$M_3(n_c)=\langle n_0\rangle[1+(\langle n_0\rangle/M)][1+2(\langle n_0\rangle/M)]\ , \tag{26c}$$

to be the representative statistics of the Poisson-driven logarithmic distribution. This turns out to be none other than the negative-binomial counting distribution,[14] with mean $\langle n_0\rangle$ and degrees-of-freedom parameter M:

$$P(n_c;T)=\frac{(n_c+M-1)!}{n_c!(M-1)!}\left[1+\frac{\langle n_0\rangle}{M}\right]^{-M}\left[1+\frac{M}{\langle n_0\rangle}\right]^{-n_c}\ , \tag{27}$$

as first shown by Quenouille.[20] Interestingly enough, the negative-binomial distribution also arises, in the context of cascade theory, as the steady-state limit of the problem of birth, death, and immigration with stationary rates.[21] The result is independent of the number of primary particles and is only valid if the death rate exceeds the birth rate; the limit thus represents a balance between the decaying cascade population and the immigration rate. The Poisson-driven Yule-Furry and the negative-binomial distributions are both two-parameter distributions.

III. EXPERIMENTS

A. The photomultiplier tube as a detector of cosmic rays

It has long been known that cosmic-ray-shower particles at ground level are registered by optical detectors such as the photomultiplier tube (PMT). The underlying reason is understood from the work of Cherenkov in 1934. A relativistic charged particle which travels at a speed exceeding the phase velocity of light in a transparent medium can induce a broadband optical shock wave with a spectral line shape predominant in the visible and ultraviolet regions of the electromagnetic spectrum.[22,23] Since this Cherenkov emission is highly directive and efficient, a single charged energetic shower component that traverses the thin photomultiplier-tube window generates a dense packet of photons that is subsequently amplified into a large anode current pulse.

Because the photomultiplier cannot resolve the individual photons from the brief Cherenkov flash, which lasts of the order of tens of picoseconds in accordance with the cosmic ray's transit time, the output signal is just the device's impulse response with an amplitude proportional to the number of Cherenkov-induced photoelectrons (if saturation effects are not considered). These large pulses in fact account for the pronounced tails in pulse-height distributions of the photomultiplier background.[24–26]

Young[27] has shown that the output current from a PMT, operated in the continuous mode in the dark, is indeed marked by substantial fluctuations that can seriously degrade the signal-to-noise ratio in a variety of experiments. As a photon counter, however, the PMT offers a significant reduction in the Cherenkov noise, since each output pulse that exceeds an adjustable threshold height yields a single count, *regardless of its excess amplitude.* The passage of a cosmic ray through the photon-counting PMT therefore registers one, *and only one,* count, although these background events may still be highly detrimental to some counting and correlation experiments. Barring other sources of PMT events, a counting distribution from the device in the dark thus provides a direct probe of the local cosmic-ray activity, and, in this capacity, the photon counter is the ideal tool for extracting its clustering properties.

Previous efforts by Young and others to characterize cosmic-ray effects at the photomultiplier tube were intended primarily for dc and mean-square current applications that do not take full advantage of pulse-height discrimination. The theoretical counting distributions considered in the previous section should provide a more appropriate and complete description of the cosmic-ray noise, since they capture the essential clustering behavior of these particles at ground level and retain their counting statistics to all orders.

B. Cosmic-ray counting experiments in space

Before examining experimental configurations at ground level in which Poisson-driven cascades play a role, it is useful to experimentally verify that the primary cosmic-ray flux above the atmosphere does indeed obey the Poisson law.

Fastie[28] conducted dark-counting experiments in space using a Schlumberger EMR type 542G-09 solar-blind PMT from the ultraviolet spectrometer aboard the Apollo 17 space-vehicle command module. He concluded that "... in lunar orbit the observed dark count varied

with spacecraft altitude and attitude, but was independent of the position of the spacecraft in lunar orbit; that is, the background signal was clearly not of solar, lunar, or earth origin." The count rate varied from 20.7 to 28.3 $\sec^{-1}$ at lunar altitudes of 26 and 312.5 km, respectively, as compared with 0.6 $\sec^{-1}$ in prelaunch laboratory tests.

The PMT background events were processed into counting probability distributions with a counting time $T=0.1$ sec, two of which are reproduced in Fig. 2. The dashed line, which represents a Poisson distribution with the same mean as the experimental data, provides a good fit in both cases. A small excess clustering is inferred from the raised tail of the experimental distributions and their associated Fano factors, which are slightly greater than unity [1.08 and 1.13 for Figs. 2(a) and 2(b), respectively]. Fastie attributes this super-Poisson effect to additive fluorescence photons from the MgF_2 window of the photomultiplier tube. We reserve a discussion of fluorescence for a later section of this paper and accept Fastie's data as confirmation of the independence of primary cosmic-ray arrivals.

C. Cosmic-ray counting experiments at ground level

1. *Models for noise in photomultiplier tubes operated in the dark*

Photomultiplier-tube background events are most often assumed to obey a simple homogeneous Poisson law, with dark-count index n_D, reflecting the presence of independently arriving events generated by thermionic emission at the photocathode and dynode stages, by radioactive elements such as ^{40}K in the window material, and by a number of other effects, some of which are discussed subsequently.[24,25,27,29] The counting distribution $P(n_D;T)$ then takes the form of Eq. (1).

However, the data at ground level do not support this simple model. Rather, it is necessary to extend this framework by incorporating cosmic-ray counts from a Poisson-driven cascade. The generalization proceeds in a twofold fashion. The cascading component of the cosmic rays has been shown to exhibit super-Poisson behavior via a counting distribution $P(n_c;T)$ that incorporates the clustered aspect of the background. A noncascading cosmic-ray component, such as the muon, is also registered at the PMT. These events are essentially independent and random and may therefore be fully absorbed in the Poisson counting distribution $P(n_D;T)$ used to describe the thermionic emission.

The generalization is provided by the independent addition of the dark index n_D with the cascade index n_c. The overall counting distribution $P(n;T)$ at ground level is then the convolution of these distributions

$$P(n;T)=P(n_C;T)\circ P(n_D;T)\ . \tag{28}$$

Their statistics up to third order are purely additive,[30] i.e.,

$$\langle n\rangle=\mu_D T+\langle n_c\rangle\ , \tag{29a}$$

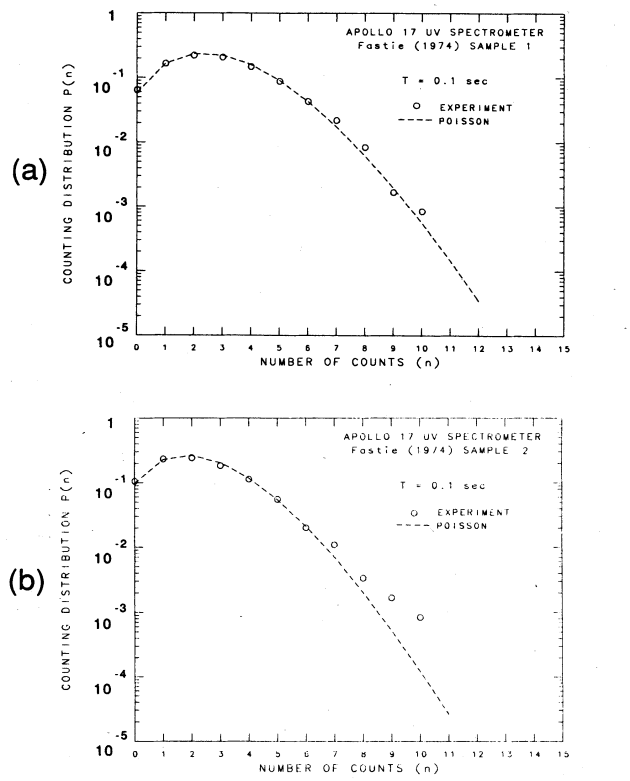

FIG. 2. (a) Sample 1 counting distribution $P(n;T)$ versus number of counts n from a Schlumberger EMR type 542G-09 photomultiplier tube in space, operated with counting time $T=0.1$ sec (data adapted from Table II of Ref. 28) The open circles represent experimental values from 5750 total samples. The mean count $\langle n\rangle=2.85$ and the Fano factor $F_n(T)=1.08$. The dashed curve is a Poisson distribution with the same mean; it represents an excellent fit to the data and confirms the independence of primary cosmic-ray arrivals. (b) Sample 2 counting distribution from the same source. In this case, the experimental mean count $\langle n\rangle=2.32$ and the Fano factor $F_n(T)=1.13$ from 5750 total samples. Fastie suggests that the excess clusters represented by the raised tail of the distribution may be caused by luminescence in the tube window.

$$V(n)=\mu_D T+V(n_c)\ , \tag{29b}$$

$$M_3(n)=\mu_D T+M_3(n_c)\ . \tag{29c}$$

The analytical form of $P(n;T)$ will clearly depend on the choice of the Poisson-driven cascade model.

Given the experimental moments obtained from the counting distribution $P(n;T)$ of a PMT operated in the dark, it is of interest to invert the relations in Eq. (29) to obtain a set of model-dependent parameters: μ_p (the primary driving rate), μ_D (the dark driving rate arising from noncascading sources), and $\langle m\rangle$ (the mean multiplication per primary). The large spatial extent of the shower and the small solid angle of acceptance of the detector lead us to expect that the parameters μ_p and $\langle m\rangle$ will not reflect the full effects of the atmospheric cascade process. Nevertheless, sufficient cosmic-ray clustering remains to control these parameters.

The inversion is facilitated by defining a convenient auxiliary parameter

$$\Gamma=[V(n)-\langle n\rangle]/[M_3(n)-V(n)] , \tag{30}$$

which is readily calculated from the statistics of $P(n;T)$. Assuming first a Poisson-driven Yule-Furry cascade, we substitute Eq. (23) into Eq. (29) to obtain

$$\langle n\rangle=\mu_D T+\mu_p T\exp(\beta) , \tag{31a}$$

$$V(n)=\mu_D T+\mu_p T\exp(\beta)[2\exp(\beta)-1] , \tag{31b}$$

$$M_3(n)=\mu_D T+\mu_p T\exp(\beta)[6\exp(2\beta)-6\exp(\beta)+1] . \tag{31c}$$

Combining the above via Eq. (30) provides a quadratic equation for the mean multiplication $\langle m\rangle=\exp(\beta)$ with the simple roots

$$\langle m\rangle=1 , \tag{32a}$$

$$\langle m\rangle=\tfrac{1}{3}[1+(1/\Gamma)] . \tag{32b}$$

Equation (32a) represents the absence of branching and is uninteresting; Eq. (32b) is, therefore, the unique solution for the nontrivial multiplicative nature of the cascade as seen by the PMT. The associated driving rates are then determined from

$$\mu_p T=[(3\Gamma)^2/2(1+\Gamma)(1-2\Gamma)](F_n-1)\langle n\rangle , \tag{32c}$$

$$\mu_D T=\{[(2-\Gamma)-(3\Gamma)F_n]/[2(1-2\Gamma)]\}\langle n\rangle , \tag{32d}$$

where F_n is the experimental Fano factor. Repeating the technique for the negative-binomial cascade, we employ Eq. (26) to yield

$$\langle n\rangle=\mu_D T+\langle n_0\rangle , \tag{33a}$$

$$V(n)=\mu_D T+\langle n_0\rangle[1+(\langle n_0\rangle/M)] , \tag{33b}$$

$$M_3(n)=\mu_D T+\langle n_0\rangle[1+(\langle n_0\rangle/M)][1+2(\langle n_0\rangle/M)] . \tag{33c}$$

Solving for the negative-binomial parameters, we obtain

$$\langle n_0\rangle=[(2\Gamma)/(1-2\Gamma)](F_n-1)\langle n\rangle , \tag{34a}$$

$$M=[(2\Gamma)/(1-2\Gamma)]^2(F_n-1)\langle n\rangle . \tag{34b}$$

Returning to the parameter of the logarithmic distribution via Eq. (25) then yields $\theta=-\ln(2\Gamma)$, so that

$$\langle m'\rangle=[\ln(2\Gamma)]^{-1}[1-(1/2\Gamma)] , \tag{35a}$$

$$\mu_p' T=\ln[1/(2\Gamma)][(2\Gamma)/(1-2\Gamma)]^2(F_n-1)\langle n\rangle , \tag{35b}$$

$$\mu_D' T=\{[1-(2\Gamma)F_n]/(1-2\Gamma)\}\langle n\rangle . \tag{35c}$$

The resemblance between Eqs. (32) and (35) is a direct consequence of the similar underlying multiplication models that are discussed in Sec. II A. We have primed the latter three parameters to minimize confusion between the two models. Graphical representations for the mean multiplications $\langle m\rangle$ and $\langle m'\rangle$ are presented in Fig. 3, as a function of Γ, for comparison. The region of physical significance is shaded and bounded on the left by infinite multiplication for $\Gamma=0$ and on the right by unity multiplication for $\Gamma=\frac{1}{2}$. This follows clearly from the expressions $\Gamma=1/[3\exp(\beta)-1]$ and $\Gamma=\frac{1}{2}\exp(-\theta)$ when $0<\beta<\infty$ and $0<\theta<\infty$, respectively. The logarithmic factor in the negative-binomial result modulates the solution in just the right way to produce a graphical trend like that for the PDYF in this domain.

2. *Experimental apparatus*

We now present the results of photon-counting experiments conducted with several different photomultipliers in the dark at ground level. A Hamamatsu type R431-S tube was operated at ambient temperature on the 13th floor of the Seeley W. Mudd building of Columbia University. It was inserted in a Hamamatsu type C1050 photon-counting base that provides preamplification, discrimination, and pulse shaping. An Ortec type 456 power supply delivered 1025 V to the PMT. The output of the PMT base was passed through a buffer amplifier (5×) and fed to a Hewlett-Packard type 5370A rate counter and a Langley-Ford type 1096 statistical photon counter. The former measures the detected mean photon count rate, whereas the latter generates the probability distribution $P(n;T)$. The experiment was controlled by a Hewlett-Packard type 9825B minicomputer.

Photon counting is a simple experimental procedure. Each sample of the counting distribution is obtained by unshuttering the photosensitive PMT cathode and recording the number of appropriately discriminated events that occur within a fixed counting time T. By repeating the procedure, enough samples are then taken to

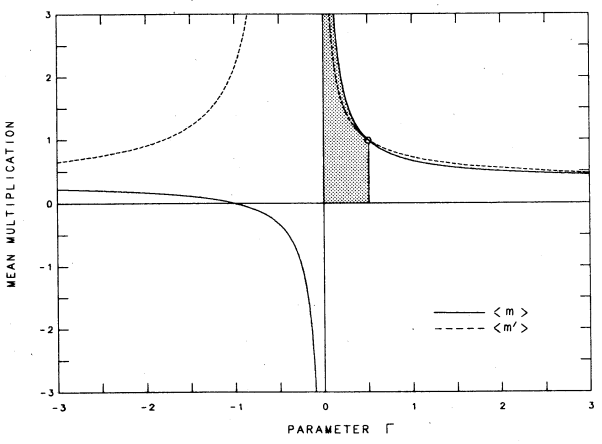

FIG. 3. Graphical dependence of the mean multiplication solutions $\langle m\rangle$ and $\langle m'\rangle$ on the experimental inversion parameter Γ. The solution represented by the solid curve is obtained if the Poisson-driven Yule-Furry (PDYF) cascade is incorporated into a model for photomultiplier background events, whereas the solution represented by the dashed curve results if the negative-binomial (NB) cascade is considered. The region of physical significance, $\frac{1}{2}>\Gamma>0$, is shaded and bounded by unity and infinite mean multiplications, respectively. The two solutions exhibit similar behavior in this region.

ensure a reliable estimate of the distribution $P(n;T)$. The total time required to collect all samples is called the experimental duration D. In the case of measurements taken in the dark, of course, the PMT is not unshuttered.

We have also operated an RCA type 8575 PMT under similar conditions using a 2-kV Kepco type 188-0030 power supply, an EGG type NA201/N quadamplifier ($8\times$), and an EGG type TR204/N discriminator. Additional data were obtained from a Schlumberger EMR type 541N-06-14 PMT being used in a study of radiation-environment effects on the star tracker for NASA's Galileo/Jupiter mission.[31]

The spectral response of all three tubes is within the Cherenkov line shape. The Hamamatsu device was selected for its high (Cs-Te) photocathode sensitivity in the ultraviolet (210 nm), whereas the other two PMT's employed bialkali materials that peak in the blue (400 nm).

3. *Counting probability distributions*

Two main sequences of experiments were carried out using the Hamamatsu tube. A discriminator setting of 1 V was used to ensure that the recorded events originate in the predynode environment. In the first sequence, the counting time T and the duration D of each experiment were fixed at 10 μsec and 10 sec, respectively. Given the duty cycle of the statistical counter (≈ 0.5) and a 5-sec processing hiatus between experiments, we were able to generate four counting distributions every minute with about 480 000 samples each. Collecting a full sequence in this set required over an hour, but we focus on the first 12 min, which are representative of the entire record.

Some of the experimental data is displayed (in histogram form) as a function of elapsed time in Fig. 4. We depict the mean count $\langle n \rangle$ of each counting distribution $P(n;T)$ in Fig. 4(a) and the associated Fano factor $F_n(T)$ in Fig. 4(b), both with a logarithmic ordinate. The total experimental background rate is ≈ 2 sec^{-1}.

The Fano factor serves as an effective tool for discerning the underlying clustering phenomena. Although it is essentially unity in nearly 70% of these experiments, the Fano factors for the remaining counting distributions are sufficiently greater than unity to signal the presence of shower events. An example is provided about halfway into the record, where there was an obvious deviation from Poisson behavior that lasted for over a minute. The shower was most intense during the counting experiment that began at the fifth minute; in a single counting time of 10 μsec there was a burst of 32 events and the Fano factor reached a value of 21. Our choice of experimental parameters is clearly sufficient to resolve the characteristic arrivals of shower particles at the detector. This behavior could not have been inferred by analyzing the evolution of the mean count alone, as is evident from the record in Fig. 4(a).

Some of the counting distributions are, however, too sparse to provide a rigorous test of the models under consideration.[32] In fact, only one super-Poisson experiment in the 12-min record was successfully fit by our models; it is shown in Fig. 5 and corresponds to 5:45 elapsed time in Fig. 4. Although a triple count occurred only once in that experiment, it was sufficient to drive the Fano factor above unity and exemplifies the vulnerability of Poisson statistics to excess clustering.

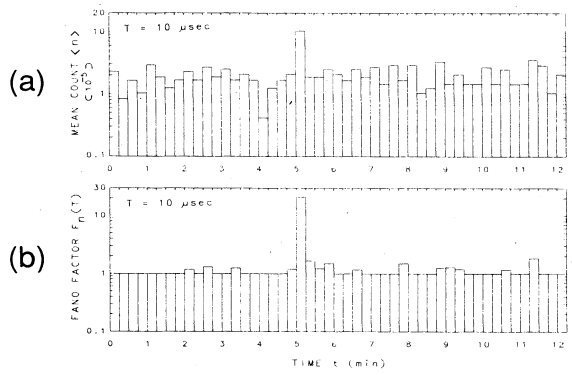

FIG. 4. (a) Mean number of events $\langle n \rangle$ (in units of 10^{-5}) versus real time t (min) registered by a Hamamatsu type R431-S PMT over a 12-min period (12/2/83, start time 17:10:00). The counting time $T=10$ μsec and the duration $D=10$ sec for each experiment. Successive experiments take place every 15 sec. The total background rate is ≈ 2 sec^{-1}. (b) Fano factor $F_n(T)$ versus real time for the same set of experiments. Note that $F_n(T)=1.0$ for about 70% of the counting distributions, indicating the complete absence of cosmic-ray clusters. It stretches to a maximum of 21 for the remaining runs, indicating the presence of bursts. The cosmic-ray contribution to the photomultiplier background can thus be generally avoided if the duration of an experiment is limited to less than tens of seconds.

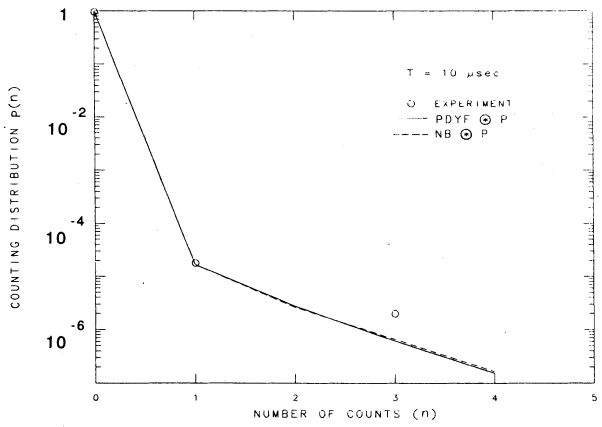

FIG. 5. Counting distribution $P(n;T)$ versus number of counts n for the Hamamatsu type R431-S PMT (12/2/83, 17:15:45) operated in the dark with count time $T=10$ μsec and duration $D=10$ sec. Open circles represent experimental values (note that $P(2)=0$); the convolution of the Poisson-driven Yule-Furry cosmic-ray cascade with a Poisson (PDYF$\circ$P) is shown as a solid curve, whereas the negative-binomial cascade convolved with a Poisson (NB$\circ$P) leads to the dashed curve. All experimental and theoretical parameters are displayed in Table I. The single triple count cluster was sufficient to drive the Fano factor to 1.5.

The resemblance between the Poisson-driven Yule-Furry and the negative-binomial descriptions of cosmic-ray showers is reflected by the near indistinguishability of the two fits in Fig. 5 and in those to follow. The convolution of the former with a Poisson distribution (PDYF $\circ$ P) is shown by the solid curve, whereas the convolution with the latter (NB$\circ$ P) is shown by the dashed-line fit. We adopt this notation for all subsequent counting distributions. Parameters have been extracted from the data for each model in accordance with Eqs. (32) and (35); these are collected in Table I.

In a second photon-counting sequence, we increased the duration D of each experiment to 1000 sec and, furthermore, changed the counting time T from 10 μsec to 59 μsec in consecutive experiments, to observe the dependence of the model parameters on T. The number of samples per counting distribution naturally decreased with increasing counting time, but with an unsubstantial loss of accuracy; at $T=59$ μsec we still obtained some 8 million samples as compared with 48 million samples at $T=10$ μsec.

We present the mean count for this sequence of experiments in Fig. 6(a) as a function of counting time T. The data exhibit reasonable linearity between $\langle n \rangle$ and T, as expected; the larger the counting period, the more the number of events from the point process that enter the counting window. The proportionality factor provides a measure of the mean rate of total background counts for this Hamamatsu tube. A linear fit to the data yields a slope of about 3.0 sec^{-1}, which accords with the estimate from Fig. 4(a).

The Fano factors in Fig. 6(b) can be compared to those of the first sequence of experiments in Fig. 4(b) (note the difference in the ordinate scales, however). The maximum value of $F_n(T)$ (6.98) occurred at $T=52$ μsec (this resulted from single dense bursts of 62 and 64 counts each), whereas the minimum Fano factor was 1.19. It is evident that, under these experimental conditions, *every* measurement in the record leads to a super-Poisson result, so the effects of cosmic-ray showers on the photomultiplier-tube background can no longer be avoided. This is a direct consequence of the increase in the duration of each experiment to $D=1000$ sec (≈ 17 min). It is longer than the entire sequence of experiments shown in Fig. 4(b), thereby unavoidably leading to the capture of cosmic-ray clusters.

The permanence of the cosmic-ray contribution throughout this data set provides an opportunity for testing the applicability of our models. We discuss two distinct examples for this tube.

TABLE I. Experimental parameters for the full counting distributions presented in Sec. III C.

Counting experiment	Fig.	Counting time T	Duration of run D	Total samples N_s	Total rate $\rightarrow 1$ $\langle n \rangle / T$ (sec^{-1})	Fano factor $F_n(T)$	Gamma factor Γ
Hamamatsu R431-S 12/02/83 17:15:45	5	10 μsec	10 sec	480 353	2.498	1.500	0.333
Hamamatsu R431-S 11/14/83 04:26:00	7	41 μsec	1000 sec	11 732 575	2.732	1.355	0.310
Hamamatsu R431-S 11/14/83 05:16:15	8(a)	44 μsec	1000 sec	10 902 318	2.952	1.538	0.142
Hamamatsu R431-S 11/14/83 05:16:15 (burst deleted)	8(b)	44 μsec	1000 sec	10 902 317	2.918	1.373	0.341
EMR 541N-06-14 09/16/77	12	40 μsec	19 min	8 192 001	58.972	1.887	0.146
RCA 8575 07/08/82 17:01:46	13	10 msec	≈ 3 d	3 499 873	149.460	2.750	0.065

Theoretical parameters extracted from fits to the data.

Counting experiment	Fig.	μ_p (sec^{-1})	$\langle m \rangle$	μ_D (sec^{-1})	μ_p' (sec^{-1})	$\langle m' \rangle$	μ_D' (sec^{-1})
Hamamatsu R431-S 12/02/83 17:15:45	5	1.405	1.333	0.625	2.026	1.233	6.241×10^{-5}
Hamamatsu R431-S 11/14/83 04:26:00	7	0.844	1.408	1.544	1.236	1.282	1.148
Hamamatsu R431-S 11/14/83 05:16:15	8(a)	0.176	2.683	2.480	0.314	2.004	2.323
Hamamatsu R431-S 11/14/83 05:16:15 (burst deleted)	8(b)	1.338	1.310	1.166	1.919	1.218	0.582
EMR 541N-06-14 09/16/77	12	6.194	2.615	42.775	10.968	1.969	37.375
RCA 8575 07/08/82 17:01:46	13	5.406	5.444	120.030	11.990	3.273	110.220

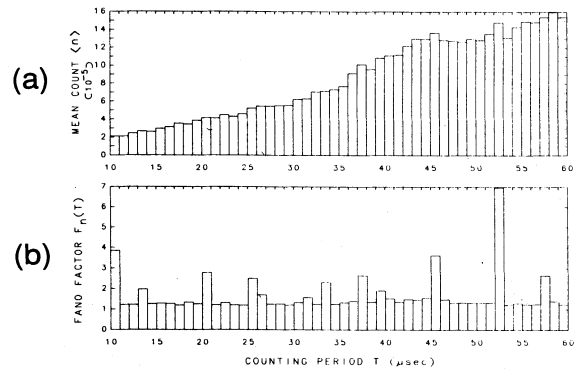

FIG. 6. (a) Mean number of events $\langle n \rangle$ (in units of 10^{-5}) versus counting time T (μsec) registered by a Hamamatsu type R431-S PMT (11/13/83, start time 19:30:00). The counting time T increases for each successive experiment beginning with $T=10$ μsec and ending with $T=59$ μsec, while the duration $D=1000$ sec throughout. The time required to collect the entire set of 50 counting distributions was ≈ 14 h. The mean count has an approximately linear dependence on T with a slope of 3 sec^{-1}. (b) Fano factor $F_n(T)$ versus counting time T for the same set of experiments. The minimum value for the Fano factor is 1.19, whereas in Fig. 4(b) it is just the unity Poisson barrier. This is a consequence of the increase in duration to 1000 sec, which results in some cosmic-ray clusters always being present in each experiment, so that it is no longer possible to avoid their effect on the photomultiplier-tube background.

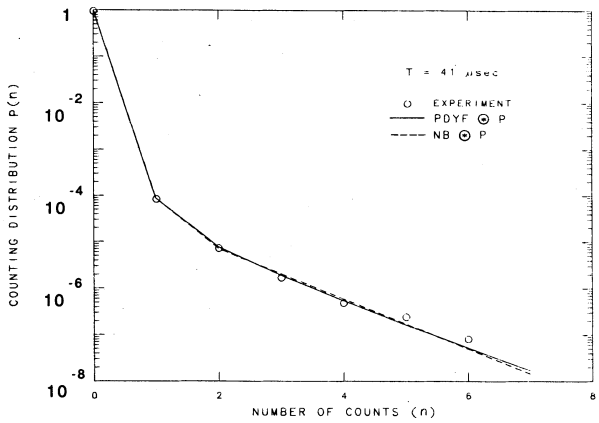

FIG. 7. Counting distribution $P(n;T)$ versus number of counts n for the Hamamatsu type R431-S PMT (11/14/83, 04:26:00) operated in the dark with counting time $T=41$ μsec and duration $D=1000$ sec. Open circles represent experimental values, whereas the solid and dashed curves represent the PDYF$\circ$P and NB$\circ$P theoretical models, respectively. All experimental and theoretical parameters are displayed in Table I. Both models provide excellent and nearly indistinguishable fits.

A typical counting distribution that lacked dense bursts is shown in Fig. 7 ($T=41$ μsec; see Fig. 6). Both models share the ability to reproduce the nearly geometric tail of the distribution with excellent precision over 7 orders of magnitude. The presence of a dense burst, on the other hand, reduces the quality of both fits substantially, as the counting distribution of Fig. 8(a) illustrates ($T=44$ μsec; see Fig. 6).

These large bursts do not, however, invalidate the theoretical approach. The cascade theory describes only the general properties of shower fluctuations and is not designed to accommodate the extremely nonstationary behavior of the dense cosmic-ray burst at $n=16$ in this data set. Indeed, it is of interest to examine the data when a singular burst such as this is removed from the counting distribution. This is illustrated in the renormalized distribution shown in Fig. 8(b). The improvement is quite dramatic and the result resembles that presented in Fig. 7 (note the difference in scale). The mean and Fano factor that result from the removal of such bursts from the data of Fig. 6 is shown in Fig. 9. Comparing these figures shows that the removal of the dense cosmic-ray activity has little effect on the mean count but significantly reduces the Fano factor. Nevertheless, $F_n(T)$ retains its super-Poisson character, as a result of the residual tails of the counting distributions.

4. *Extraction of model parameters*

The uniformity of this revised data set encouraged us to attempt to extract the stationary properties of our three model parameters. The total background-count rate is decomposed into a cosmic-ray primary rate and a dark rate from other sources at the detector. The last parameter carries the multiplicative strength of the atmospheric cascade. The theoretical parameters corresponding to the two models, $\{\mu_p,\langle m\rangle,\mu_D\}$ and $\{\mu_p',\langle m'\rangle,\mu_D'\}$, are given by Eqs. (32) and (35), respectively. These were extracted from each counting distribution represented in Fig. 9 and are displayed in Figs. 10(a)–10(c) and 11(a)–11(c) for the Poisson-driven Yule-Furry and negative-binomial models, respectively.

One immediate feature of the results is the stability of the mean multiplication that is obtained from both models over the entire range of counting times. From a mathematical point of view, the similarity in the magnitude of $\langle m\rangle$ and $\langle m'\rangle$ (both are ≈ 1.2) results from the proximity of the inversion parameter ($\Gamma \approx \frac{1}{3}$) to the region of convergence of the two solutions in Fig. 3.

Whatever small variation exists in the full background rate must, therefore, be apportioned to the primary and dark rates. Those for the PDYF$\circ$P are about the same order of magnitude ($\mu_p,\mu_D \approx 1.0\ \text{sec}^{-1}$), whereas the NB$\circ$P model places a slightly greater emphasis on the primary rate ($\mu_p' \approx 1.2\ \text{sec}^{-1}$) with a corresponding decrease in the dark rate ($\mu_D' \approx 0.7\ \text{sec}^{-1}$). This comparative reduction in μ_D' has the effect of reducing the fitting efficiency of the NB$\circ$P model, for its dark-rate estimate is more likely to be driven below zero on occasion, and thus yield an unacceptable solution. This is evident from the gaps in the histogram records of Figs. 10 and 11 (the PDYF$\circ$P model successfully fit 49 of 50 experiments, while the NB$\circ$P model could not accommodate five additional cases).

From the above parameters, we find the total fluctuation of cosmic-ray particles at ground level in this range of counting times to be about $\mu_p\langle m\rangle \approx 1.2\ \text{sec}^{-1}$ and

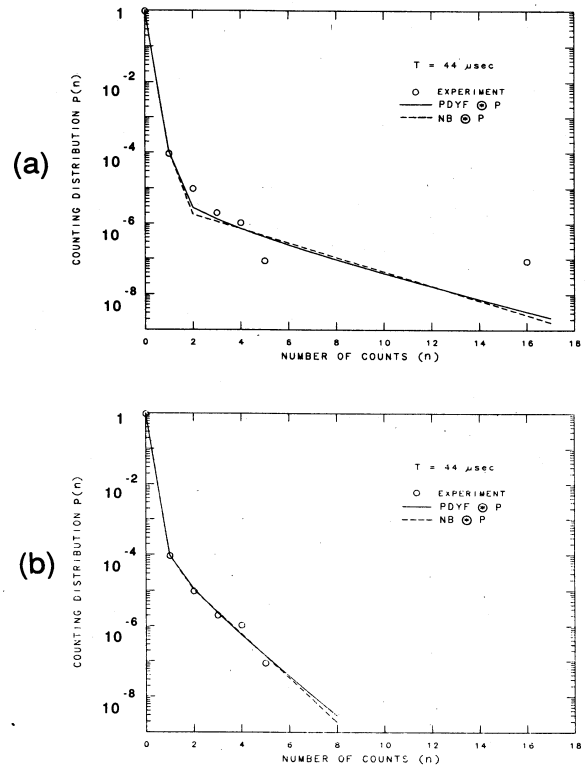

FIG. 8. (a) Counting distribution $P(n;T)$ versus number of counts n for the Hamamatsu type R431-S PMT (11/14/83, 05:16:15) operated in the dark with counting time $T=44$ μsec and duration $D=1000$ sec. The open circles represent experimental values, whereas the solid and dashed curves represent the PDYF⊙P and NB⊙P theoretical models, respectively. All experimental and theoretical parameters are displayed in Table I. Note the presence of a dense cosmic-ray burst at $n=16$ which reduces the quality of the fit. (b) Counting distribution for the same experiment after removal of the singular dense shower at $n=16$ and renormalization of the data. Now note the similarity to Fig. 7. The Fano factor decreased from 1.54 to 1.38.

$\mu_p'\langle m'\rangle \approx 1.44$ sec^{-1} for the two models. These observed rates are an order of magnitude higher than that which is expected from an estimated sea-level flux of 1.0 cm^{-2} min^{-1} (Ref. 27) through the 2.5-cm Hamamatsu photocathode (i.e., 0.1 sec^{-1}). The discrepancy may arise from the superior resolution of this PMT operated in the photon-counting mode, which can detect low-height Cherenkov pulses.

5. *Counting probability distributions for other PMT's*

These observations are complemented by two additional counting distributions obtained with PMT's other than the Hamamatsu. The former used a counting period similar to that employed in our second sequence of experiments ($T=40$ μsec, duration $D=19$ min) with the Schlumberger EMR type 541N-06-14 PMT. This PMT is similar to that to be used in the now pending NASA/JPL Galileo mission to Jupiter. The distribution, which is shown in Fig. 12, resembles that for the Hamamatsu PMT shown in Fig. 7, except that larger clusters are observed.

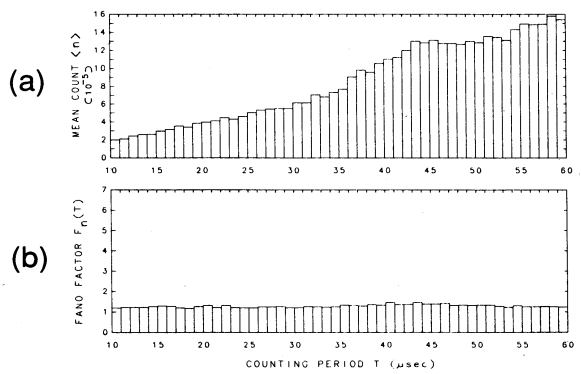

FIG. 9. (a) Mean count $\langle n\rangle$ (in units of 10^{-5}) and (b) Fano factor $F_n(T)$ versus counting time T (μsec) for the sequence of experiments illustrated in Fig. 6, after removal of large count numbers resulting from intense brief cosmic-ray bursts. The mean count was not significantly affected, but the occasional high peaks in the Fano factor that are prevalent in Fig. 6 are eliminated. Nevertheless, the counting distributions remain super-Poisson, with $F_n(T)\approx 1.3$, in the range of counting times displayed. The variation of T does not contribute to the raising of the Fano factor above unity; rather, this results from the increased experimental duration D.

The final counting distribution, presented in Fig. 13, represents one of two similar experiments carried out with an RCA type 8575 tube. The counting time and duration were especially long ($T=10$ msec, $D\approx 3$ d). Although the full distribution extended to the count number $n=137$, it was curtailed at $n=50$ and renormalized to increase clarity, but without loss of essential information.

This experiment is appealing because it facilitates an

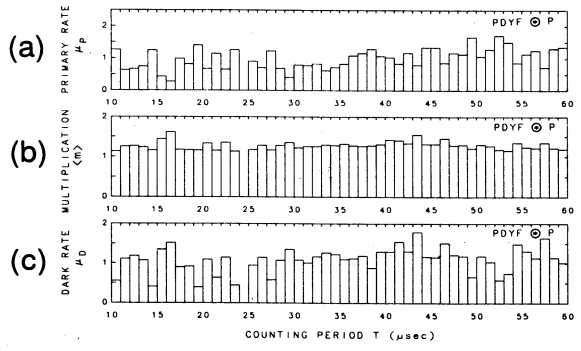

FIG. 10. (a) Primary cosmic-ray driving rate μ_p (sec^{-1}), (b) mean multiplication $\langle m\rangle$ and (c) dark (noncascading) driving rate μ_D (sec^{-1}), versus counting time T. These parameters were extracted from the sequence of experiments shown in Fig. 9 via the PDYF⊙P model for background events. They do not vary substantially over the entire range of counting times displayed. Only one experiment (For $T=24$ μsec) out of 50 was not able to be fit by the model.

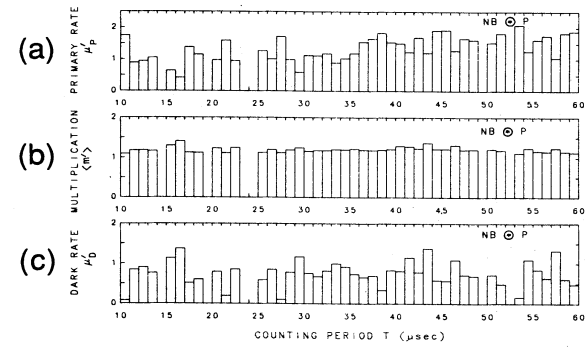

FIG. 11. (a) Primary cosmic-ray driving rate μ_p' ($\sec^{-1}$), (b) mean multiplication $\langle m' \rangle$, and (c) dark (noncascading) driving rate μ_D' ($\sec^{-1}$), versus counting period T. These parameters were extracted from the sequence of experiments shown in Fig. 9 via the NB∘P model background events. They do not vary substantially over the range of counting times displayed. A total of six counting distributions out of 50 were not able to be fit by this model.

identification of the two components of each model . For low count numbers, the shape of the distribution is inherited primarily from the Poisson law of the noncascading events ($\langle n_D \rangle = \mu_D T \approx 1.2$, whereas $\langle n_p \rangle = \mu_p T \approx 0.054$). On the other hand, the quasigeometric tail beyond $n = 5$ is characteristic of the appropriate PDYF and negative-binomial distributions; it provides a telltale signature of cosmic-ray clusters at the detector. This dual behavior is quite adequately captured by the models we have considered.

We also remark on the manner of decomposition of the total background rate: in Table I it is shown that the dark rate for this counting distribution received the largest share in such a way as to maintain the primary rate estimate within an order of magnitude of those for the Hamamatsu tube experiments. This is not unreasonable since it is likely that noncascading sources (such as thermionic emission) and discriminator adjustments will vary from one experimental setup to another.

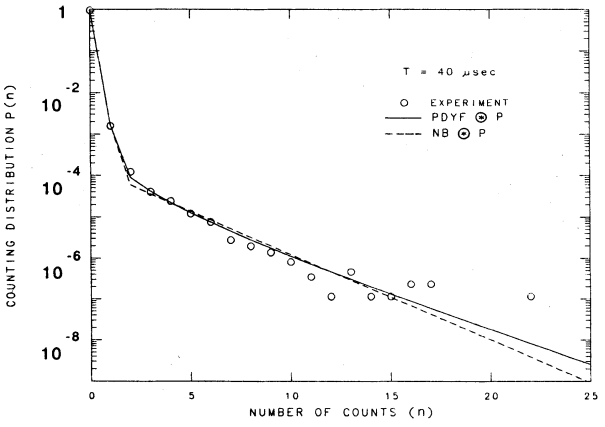

FIG. 12. Counting distribution $P(n;T)$ versus number of events n for the Schlumberger EMR type 541N-06-14 PMT designed for the NASA/JPL Galileo mission (9/16/77, Base line B-1 experiment) operated in the dark with counting period $T = 40$ μsec and duration $D = 19$ min. Open circles represent experimental values. Solid and dashed curves represent the PDYF∘P and NB∘P theoretical models, respectively. The experimental and theoretical parameters are displayed in Table I. This distribution resembles that for the Hamamatsu PMT displayed in Fig. 7 except that larger clusters are observed.

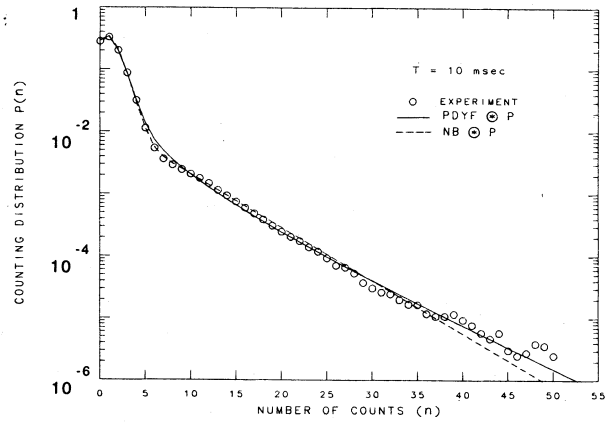

FIG. 13. Counting distribution $P(n;T)$ versus number of events n for the RCA type 8575 PMT (7/8/82, 17:01:46) operated in the dark with counting time $T = 10$ msec and duration $D \approx 3$ d. Open circles represent experimental values. The solid and dashed curves represent the PDYF∘P and NB∘P theoretical models, respectively. All experimental and theoretical parameters are displayed in Table I. The underlying Poisson distribution for noncascading sources is clearly evident for low count numbers ($n \leq 5$), whereas the characteristic tail from the Poisson-driven cascade counting distributions is observed for large count numbers ($n \geq 5$). Both models capture this dual behavior with remarkable precision.

D. Interevent-time probability density functions

The experimental counting distribution $P(n;T)$ is an important statistical measure of a point process. The process of counting, however, forsakes a knowledge of the occurrence times of the individual events and, therefore, provides only a partial characterization of the entire point process. Another window on this information is the probability distribution $P(\tau)$ of the interevent times, which is constructed experimentally by recording a histogram for the temporal separations of adjacent pulses that are properly discriminated (see the discussion on pulse discrimination in Sec. III A). For the homogeneous Poisson point process, this distribution follows the simple exponential law $P(\tau) = \mu \exp(-\mu\tau)$, where μ is the constant driving rate of the process.[6,7]

In Fig. 14(a) we present $P(\tau)$ for the RCA type 8575 PMT operated in the dark. On these semilogarithmic coordinates, the experimental distribution may indeed be well approximated by a linear trend for large interevent times, but this Poisson description fails for $\tau \leq 0.01$ sec. The deviation can be scrutinized by a double-logarithmic presentation of this same data, as shown in Fig. 14(b). A similar distribution has been obtained with the

Hamamatsu type R431-S PMT, as shown in Fig. 15.

A sharp peak appears in Fig. 14(b) at $\tau \approx 0.5$ μsec; this same phenomenon occurs, and is especially pronounced, in Fig. 15 at $\tau \approx 0.12$ μsec. This feature is attributed to brief but intense bursts of evenly spaced cosmic-ray events of unknown origin, which drive the Fano factor in counting experiments well above unity. These peaks permit us to estimate the typical intracluster event spacing. Since the smallest counting periods in our counting experiments ($T = 10$ μsec) are well in excess of the intracluster separation, it is clear that many of these events are indeed captured.

The broader tails of the two distributions (at the largest values of τ) are exponential and reflect intercluster separations arising from the cascade's primary (Poisson) process. Additional counts from noncascading sources at the PMT are also present, but these do not alter the exponential character of this tail since they are also random events. The quenching of both distributions below $\tau \approx 100$ nsec arises from the limited electronic resolution of the detectors. Typical pulse durations (full-width half maximum) for the Hamamatsu system are rated at about 25 nsec.

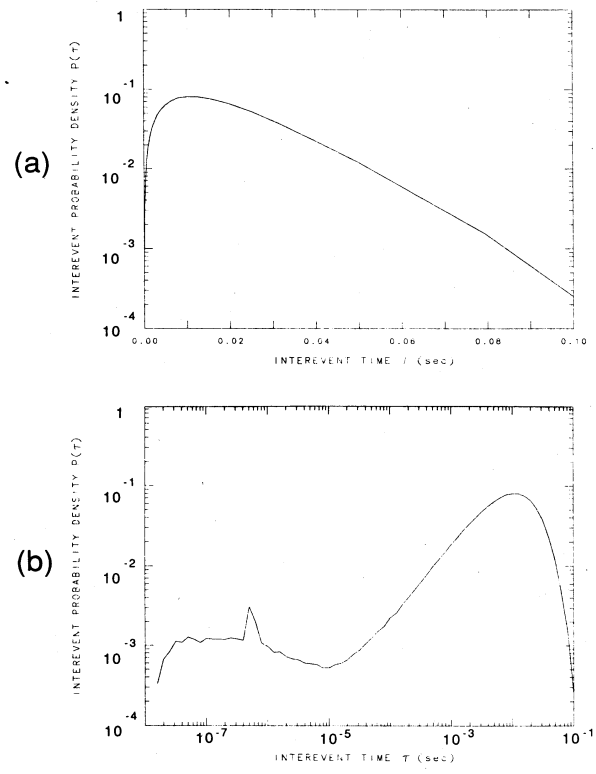

FIG. 14. (a) Interevent probability density $P(\tau)$ versus interevent time τ (sec) for background counts in a RCA type 8575 PMT, on semilogarithmic coordinates. The approximately exponential dependence for $\tau > 0.01$ sec reflects Poisson-distributed arrival times. The data set was collected on 7/19/82, at an 18:59:35 start time, and contain 881 002 samples. (b) The same data presented in a double-logarithmic format. The peak at $\tau \approx 0.5$ μsec reflects cosmic-ray intercluster event spacings. Even the smallest counting period used in our counting experiments ($T = 10$ μsec) is sufficiently large to capture these clustered events.

E. Other sources of dark events in the photomultiplier tube

The phenomena of afterpulsing and luminescence, which are known to be important sources of spurious counts in certain photomultiplier tubes, have not been incorporated into our models. Since these are primarily tube-dependent effects, the introduction of further branching steps to the mathematical formulation may not always be necessary.

Afterpulsing is known to arise in photomultipliers from ion bombardment of the cathode and initial dynodes.[24,29] These charged agents result from the ionization of residual and leakage gases (such as hydrogen, helium, and nitrogen) during electromultiplication. The process is governed by the ion transit time, which is broadly distributed (even if afterpulsing from the dynodes is eliminated by proper discrimination) since it depends on the mass of the ionized species and its path length back to the photocathode.

A simple estimate of the afterpulsing probability $P_a(T)$ per photocathode event can be obtained by considering a cascade of Poisson primaries with a Bernoulli law for the creation of secondary afterpulses. Using a laser source of Poisson photons (to render the dark-rate contribution negligible) and conducting photon-counting experiments at $T = 1$ μsec and $D = 0.4$ sec (to enable cosmic-ray effects to be excluded from most of the experiments), Teich and Saleh[33] estimated that $P_a(1\ \mu\text{sec}) \approx 1.6 \times 10^{-3}$ for the Hamamatsu tube. For larger counting times, an enhancement of $P_a(T)$ is expected, since more afterpulses are likely to be captured by the increased time window.

Even so, this is not sufficient to account for the very

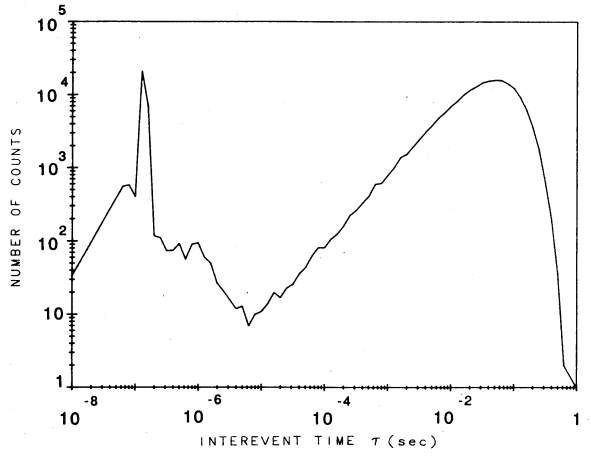

FIG. 15. Interevent probability density $P(\tau)$ versus interevent time τ (sec) for background counts in a Hamamatsu type R431-S PMT, on double-logarithmic coordinates. The distribution resembles that of Fig. 14(b). The pronounced feature arising from clustered cosmic-ray effects is evident at $\tau \approx 0.13$ μsec. The data set was collected on 9/7/83 and contains 500 000 samples.

gradual decrease in probability between adjacent counts beyond $n=1$ in all our experimental distributions; it is typically shallower than that required by the above estimate. We conclude that the afterpulsing contribution is not crucial and need not be considered in our models.

Luminescence can arise from the excitation and relaxation of molecular states in the faceplate material of the PMT, and has been studied extensively in connection with the effects of the radiation environment on spaceborne photomultiplier tubes.[34–37] Unlike Cherenkov photons, which are copiously produced but cannot be individually resolved at the detector, the less numerous luminescence photons are emitted during the comparatively long molecular relaxation times and may thus be registered as individual events. In fluorescence decay, this deexcitation commonly occurs from over a few to hundreds of microseconds, whereas in phosphorescence decay times may span from minutes to days. Of the two processes, the former is likely to be most significant to our counting experiments because its decay parameter can be well accommodated within the chosen counting times.

A statistical estimate of fluorescence noise is very difficult to obtain, unless the correlation between cosmic rays and fluorescence photons at the detector is known. This relationship cannot be deduced following a photon-counting experiment because knowledge of the occurrence times and pulse heights of individual events is lost. For this reason we cannot totally exclude fluorescence from our experimental measurements, although arguments against its dominance can be set forth.

If cosmic-ray particles were completely divorced from fluorescence emissions, the latter would simply add to the uniform background of random events, which is naturally incorporated into our models via the dark-rate parameter μ_D. A strong correlation between the two phenomena, on the other hand, would imply that a cosmic-ray count is closely followed by fluorescence events, thus falsely enhancing the shower clustering properties.

However, recent numerical simulations by Howell and Kennel of NASA (Ref. 35) have shown that existing correlations between Cherenkov and fluorescence photons in the PMT window are substantially reduced en route to detection at the photocathode. According to their simulated bivariate distribution, the latter may even at times appear without the presence of the former. "This," the authors suggest, "may be largely attributed to the directed nature of the Cherenkov radiation, in which photons exit the window with little or no internal reflection, but the fluorescence photons, in their more random flights, eventually strike the photocathode either directly or after reflection."

Some evidence in favor of this view may be gathered from our data. For instance, the experimental interevent time distributions shown in Figs. 14(b) and 15 reach local minima precisely within the temporal region associated with fluorescence photon arrivals (1–100 μsec). This is particularly true of the Hamamatsu tube, perhaps because its solar-blind response reduces fluorescence in the visible regime. Strong correlations would most certainly yield an enhancement in this emission-time window.

The small excess clustering that exists in the Apollo 17 counting distributions from space with very long counting times (see Fig. 2) also supports the above interpretation, especially since the MgF_2 window of the associated PMT fluoresces more efficiently than the SiO_2 and glass materials used by the other photomultipliers.[37]

We believe fluorescence is not sufficient to fully account for the observed geometric feature that is so well described by our models (see Fig. 13). Nevertheless, future experiments employing point-process detectors in conjunction with pulse-height analyzers would more precisely elucidate the contribution of fluorescence noise to the clustered photomultiplier background.

IV. CONCLUSION AND DISCUSSION

We have shown that cosmic-ray-shower fluctuations at ground level can be effectively represented by the Poisson-driven Yule-Furry or the negative-binomial (Poisson-driven logarithmic) two-parameter counting probability distributions. The agreement between data and theory determined with photomultiplier tubes operated in the dark is remarkable, given the simplicity of the underlying pure-birth cascade model. The mathematical basis for the success of the theory lies in the presence of mean-square excess fluctuations in the variance of the multiplication statistics, of which the Yule-Furry and the logarithmic distributions are fundamental examples. In order to extract the cosmic-ray-shower component from the PMT data, we found it necessary to formulate a more precise description of photomultiplier background events by combining the Poisson-driven cascades with an independent Poisson random variable that summarizes other count sources at the detector.

Finally, we note that cosmic-ray clusters are particularly deleterious to some counting experiments. We have shown that cosmic-ray clusters can, in fact, be avoided in photon-counting experiments by restricting the counting duration to less than tens of seconds. The background events can then be described by a simple Poisson counting distribution with a very low mean (which is just a Bernoulli distribution when only 0 or 1 counts are observed). This is particularly useful for applications that seek to determine counting statistics which are sensitive to excess clustering. One important example is the detection of stationary photon-number squeezed light, as recently reported by a number of authors,[33,38–40] since the superposition of super-Poisson cosmic-ray counts at the phototube may destroy the nonclassical observable. In general, if photomultiplier tubes are used in photon-counting experiments that cannot be conducted at short durations, cosmic-ray clusters may pose a significant limitation. The background models we have presented will then provide a useful analytical point of departure.

ACKNOWLEDGMENTS

This work was supported by the National Science Foundation and by the Joint Services Electronics Program at Columbia University. We are grateful to members of the NASA Goddard Institute for Space Studies for providing access to computer and plotting facilities, and for assistance in locating various NASA documents. William Mindel is also acknowledged for computer-related support. We appreciate greatly the participation of Sridhar Anandakrishnan, Ned Peirce, and Todd Larchuk in various phases of the experiments.

APPENDIX A: RELATIONSHIP BETWEEN YULE-FURRY AND LOGARITHMIC COUNTING STATISTICS

The statistical behavior of logarithmic counting statistics was shown in Sec. II A to resemble that of the pure-birth (Yule-Furry) model. The purpose of this appendix is to present a connection between the two counting distributions.

For a general discrete probability distribution $P(x)$, we consider the expectation

$$\left\langle \frac{x}{\langle x \rangle} \right\rangle = \sum_{x=0}^{\infty} \frac{x}{\langle x \rangle} P(x) = 1 , \tag{A1}$$

which is clearly normalized. This leads us to view the summed expression above as a probability transformation of the type

$$P_B(x) = [x/\langle x_A \rangle] P_A(x) , \tag{A2}$$

from which the auxiliary condition

$$\langle x_B \rangle = F_A + \langle x_A \rangle \tag{A3}$$

may be obtained, where F_A is the Fano factor, or variance-to-mean ratio, of the original distribution.

It is evident from the construction of Eq. (A2) that $P_B(x)$ is zero when $x=0$, although this need not be true for $P_A(x)$. The former distribution may thus belong to the class of unit-shifted counting distributions, whose members can represent cascades in which the primary particle is included along with its offspring (as discussed in Sec. II A).

If $P_A(x)$ is the Poisson distribution, we employ Eqs. (1) and (3) to evaluate Eqs. (A2) and (A3):

$$P_B(x) = \langle x_A \rangle^{x-1} \exp(-\langle x_A \rangle)/(x-1)!, \quad x \geq 1 , \tag{A4a}$$

$$\langle x_B \rangle = 1 + \langle x_A \rangle . \tag{A4b}$$

This is just a unit-shifted version of the Poisson input, which can be easily verified by comparison with Eq. (5).

On the other hand, if $P_A(x)$ is the logarithmic distribution, then with the aid of many of Eqs. (7)–(13) we in fact obtain the Yule-Furry, or shifted Bose-Einstein, statistic:

$$P_B(x) = \exp(-\beta)[1-\exp(-\beta)]^{x-1}, \quad x \geq 1 , \tag{A5a}$$

as long as

$$\langle x_B \rangle = 1 + \theta \langle x_A \rangle, \quad \text{or } \theta = \beta . \tag{A5b}$$

The simplicity of the transformation that links the Yule-Furry and logarithmic distributions is reflected by their shared mathematical properties.

We may recast Eq. (A2) into equivalent relations in the domain of generating functions. The most compact result is obtained via the probability-generating function (PGF), which is defined as

$$G(z) \equiv \langle z^x \rangle = \sum_{x=0}^{\infty} z^x P(x) . \tag{A6}$$

Applying Eq. (A6) to Eq. (A2) and using

$$G_B^{(s)}(z) = z G_B(z) , \tag{A7}$$

which relates the PGF's of the shifted and unshifted counting distributions, respectively, we obtain

$$G_B(z) = \frac{1}{\langle x_A \rangle} \frac{d}{dz} G_A(z) , \tag{A8a}$$

and its inverse

$$G_A(z) = \langle x_A \rangle \int_0^z G_B(z) dz . \tag{A8b}$$

From Eq. (A8b) we can see that the logarithmic PGF behaves like an unbounded cumulative version of the (unshifted) Bose-Einstein PGF. The moments of these two distributions can be linked to all orders by evaluating Eq. (A8) at $z = \exp(-s)$ to obtain relations for the moment-generating function $Q(s)$, whose properties are given by Eqs. (B1) and (B2) of Appendix B.

APPENDIX B: THIRD-ORDER MOMENTS FOR A CASCADED PROCESS

It is well known that the nth ordinary moment of a general counting distribution $P(x)$ may be obtained from its moment-generating function (MGF) (Ref. 14),

$$Q_x(s) \equiv \langle \exp(-sx) \rangle = \sum_{x=0}^{\infty} \exp(-sx) P(x) , \tag{B1}$$

by successive differentiation according to

$$\langle x^n \rangle = (-1)^n \frac{\partial^n}{\partial s^n} Q_x(s) \bigg|_{s=0} \quad \text{for all } n . \tag{B2}$$

Alternatively, it is oftentimes more convenient to employ the semi-invariant or cumulant-generating function (CGF)

$$K_x(s) \equiv \ln[Q_x(s)] , \tag{B3}$$

which yields the mean $\langle x \rangle$, variance $V(x)$, and third central moment $M_3(x)$ directly:

$$\langle x \rangle = -\frac{\partial}{\partial s} K_x(s) \bigg|_{s=0} , \tag{B4a}$$

$$V(x)=\frac{\partial^2}{\partial s^2}K_x(s)\bigg|_{s=0}, \tag{B4b}$$

$$M_3(x)=-\frac{\partial^3}{\partial s^3}K_x(s)\bigg|_{s=0}. \tag{B4c}$$

This simple pattern does not persist beyond third order, however.

Consider a primary process p characterized by the MGF $Q_p(s)$, whose members independently initiate a branching process resulting in an overall multiplication m described by $Q_m(s)$. The moment-generating function of the overall compound process mixes the above via

$$Q_c(s)=Q_p(-\ln Q_m(s)), \tag{B5}$$

which, using Eq. (B3), can be rewritten in terms of the associated CGF's as

$$K_c(s)=K_p(-K_m(s)). \tag{B6}$$

Differentiating both sides according to Eq. (B4), and expanding via the chain rule, leads to the general relations

$$\langle n_c\rangle=\langle p\rangle\langle m\rangle, \tag{B7a}$$

$$V(n_c)=V(p)\langle m\rangle^2+\langle p\rangle V(m), \tag{B7b}$$

$$M_3(n_c)=M_3(p)\langle m\rangle^3+3V(p)\langle m\rangle V(m)+\langle p\rangle M_3(m), \tag{B7c}$$

which may be applied to any simple compound process where a primary counting distribution $P(p)$ drives a multiplication counting distribution $P(m)$.

[1]B. B. Rossi, *Cosmic Rays* (McGraw-Hill, New York, 1964).

[2]Traces of protons, deuterons, tritons, alpha particles, and heavier nuclei have also been detected at ground level, as discussed by P. C. M. Yock, Phys. Rev. D **34**, 698 (1986).

[3]G. R. Smith, M. Ogmen, E. Buller, and S. Standil, Phys. Rev. Lett. **50**, 2110 (1983).

[4]H. J. Bhabha and W. Heitler, Proc. R. Soc. London **A159**, 432 (1937).

[5]J. F. Carlson and J. R. Oppenheimer, Phys. Rev. **51**, 220 (1937).

[6]B. E. A. Saleh, *Photoelectron Statistics* (Springer, New York, 1978).

[7]D. L. Snyder, *Random Point Processes* (Wiley, New York, 1975).

[8]U. Fano, Phys. Rev. **72**, 26 (1947).

[9]W. Furry, Phys. Rev. **52**, 569 (1937).

[10]G. U. Yule, Phil. Trans. R. Soc. London **B213**, 21 (1924).

[11]N. Arley, *On the Theory of Stochastic Processes and Their Application to the Theory of Cosmic Radiation* (Wiley, New York, 1943).

[12]S. K. Srinivasan, *Stochastic Theory and Cascade Processes* (Elsevier, New York, 1969).

[13]K. Shimoda, H. Takahasi, and C. Townes, J. Phys. Soc. Jpn. **12**, 686 (1957).

[14]E. Parzen, *Stochastic Processes* (Holden-Day, San Francisco, 1962).

[15]W. Shockley and J. R. Pierce, Proc. IRE **26**, 321 (1938).

[16]R. E. Burgess, J. Phys. Chem. Solids **22**, 371 (1961).

[17]C. C. Shih, Phys. Rev. D **34**, 2710 (1986).

[18]K. Matsuo, M. C. Teich, and B. E. A. Saleh, J. Math. Phys. **25**, 2174 (1984).

[19]M. C. Teich, K. Matsuo, and B. E. A. Saleh, IEEE Trans. Electron Devices **ED-33**, 1475 (1986).

[20]M. H. Quenouille, Biometrics **5**, 162 (1949).

[21]M. S. Bartlett, *An Introduction to Stochastic Processes* (Cambridge University Press, Cambridge, England, 1966).

[22]J. V. Jelley, *Čerenkov Radiation and its Applications* (Pergamon, New York, 1958).

[23]J. D. Jackson, *Classical Electrodynamics* (Wiley, New York, 1975).

[24]A. T. Young, Appl. Opt. **8**, 2431 (1969).

[25]A. G. Wright, J. Phys. E **16**, 300 (1983).

[26]R. L. Jerde, L. E. Peterson, and W. Stein, Rev. Sci. Instrum. **38**, 1387 (1967).

[27]A. T. Young, Rev. Sci. Instrum. **37**, 1472 (1966).

[28]W. G. Fastie, Apollo 17 UV Spectrometer Experiment (S-169), final report, Addendum C, NASA Contract No. NAS 9-11528, 1974.

[29]R. W. Engstrom, *RCA Photomultiplier Handbook (PMT-62)* (RCA Electro-Optics and Devices, Lancaster, PA, 1980).

[30]It is well known that a random variable formed by the addition of N independent random variables has a moment-generating function given by the product of the individual moment-generating functions (Ref. 14):

$$Q_x(s)=\prod_{j=1}^{N}Q_j(s).$$

This can be rewritten as

$$Q_x(s)=\exp\left[\sum_{j=1}^{N}\ln Q_j(s)\right],$$

which, with the help of Eq. (B3), becomes

$$K_x(s)=\sum_{j=1}^{N}K_j(s).$$

It follows immediately from the differentiation properties of the cumulant-generating function provided in Eq. (B4) that the means, variances, *and* third central moments are additive, i.e.,

$$M_3(x)=\sum_{j=1}^{N}M_3(x_j).$$

[31]J. T. Tavolacci and M. C. Teich (unpublished).

[32]This reflects the fact that each model is governed by three free parameters, so at least three independent data points per counting distribution are required for a fit.

[33]M. C. Teich and B. E. A. Saleh, J. Opt. Soc. Am. B **2**, 275 (1985).

[34]B. E. A. Saleh, J. T. Tavolacci, and M. C. Teich, IEEE J. Quantum Electron. **QE-17**, 2341 (1981).

[35]L. W. Howell and H. F. Kennel, NASA Technical Report No. 2337, 1984.

[36]W. Viehmann and A. G. Eubanks, NASA Report No. TN D-8147, 1976.
[37]W. Viehmann, A. G. Eubanks, G. F. Piper, and J. H. Bredekamp, Appl. Opt. **14**, 2104 (1975).
[38]P. R. Tapster, J. G. Rarity, and J. S. Satchell, Europhys. Lett. **4**, 293 (1987).
[39]S. Machida, Y. Yamamoto, and Y. Itaya, Phys. Rev. Lett. **58**, 1000 (1987).
[40]L. A. Wu, H. J. Kimble, J. L. Hall, and H. Wu, Phys. Rev. Lett. **57**, 2520 (1986).